JGR Atmospheres

RESEARCH ARTICLE
10.1029/2019JD030857

Polarimetric Radar Convective Cell Tracking Reveals Large Sensitivity of Cloud Precipitation and Electrification Properties to CCN

Jiaxi Hu[1], Daniel Rosenfeld[2], Alexander Ryzhkov[1], Dusan Zrnic[1,5], Earle Williams[4], Pengfei Zhang[1], Jeffrey C. Snyder[1,5], Renyi Zhang[3], and Richard Weitz[3]

[1]University of Oklahoma, and NOAA/OAR National Severe Storms Laboratory, Cooperative Institute for Mesoscale Meteorological Studies, Norman, OK, USA, [2]Department of Atmospheric Sciences, The Hebrew University of Jerusalem, Jerusalem, Israel, [3]Department of Atmospheric Sciences, Texas A&M University, College Station, TX, USA, [4]Massachusetts Institute of Technology, Cambridge, MA, USA, [5]NOAA/OAR/National Severe Storms Laboratory, Norman, Oklahoma, USA

Abstract Hypotheses have been proposed for decades about the effect of activated cloud condensation nuclei (CCN) on delaying the warm rain process, invigorating deep convective cloud vertical development, and enhancing mixed-phase processes. Observational support has been only qualitative with mixed results due to the lack of regional measurements of CCN concentration (N_{CCN}), while simulations have not produced a robust consensus. Quantitative assessments of these relationships became possible with the advent of N_{CCN} retrievals from satellites; when combined with measurements by polarimetric radar and Lightning Mapping Array (LMA), tracking convective cells observed on radar and examining precipitation properties throughout the cells' life cycle has permitted the study of the impact of N_{CCN} on cloud and precipitation characteristics. We composited more than 2,800 well-tracked cells in the Houston region and stratified them by N_{CCN}, convective available potential energy (CAPE), and urban/rural locations. The results show that increased N_{CCN} invigorates the convection until saturation near N_{CCN} = 1,000 cm^3; increasing N_{CCN} from ~400 to an optimum of ~1,000 cm^3 increases lightning activity by an order of magnitude. A further increase in CCN decreases lightning rates. Adding CAPE enhances lightning only under low N_{CCN} (e.g., less than 500 cm^3). The presence of the urban area enhances lightning for similar N_{CCN} concentrations, although this applies mainly under low N_{CCN} conditions. The urban heat island as manifested by cloud base height cannot explain this observation. It is suspected that the urban ultrafine aerosols contribute to the storm electrification.

Plain Language Summary Deep convective clouds are propelled by rising air currents and are composed of cloud droplets that nucleate on CCN aerosols. Isolating the effects of CAPE and N_{CCN} on cloud properties has been an unresolved challenge. Tracking the time-height evolution of a large number of individual summer convective storm cells in the Houston area under various CAPE and N_{CCN} shows their relations to the storm's dynamics, precipitation, and electrification processes. The results show that increased N_{CCN} invigorates the convection, produces larger hydrometeors, and enhances lightning. Variability in N_{CCN} was found to be more important than variability in CAPE, cloud base height, and wind shear in explaining the variability of the vigor and electrification of deep convective clouds in the study area.

Key Points:
- Increased CCN invigorates convection, produces larger hydrometeors, and enhances lightning
- CCN invigoration effect saturates near N_{CCN} = 1,000 cm^3 in an environment with similar CAPE
- CCN is more important than CAPE in explaining the variability of the vigor and electrification of storms after convection is initiated

Supporting Information:
- Supporting Information S1

Correspondence to:
J. Hu,
jiaxi.hu@noaa.gov

Citation:
Hu, J., Rosenfeld, D., Ryzhkov, A., Zrnic, D., Williams, E., Zhang, P., et al. (2019). Polarimetric radar convective cell tracking reveals large sensitivity of cloud precipitation and electrification properties to CCN. *Journal of Geophysical Research: Atmospheres*, *124*, 12,194–12,205. https://doi.org/10.1029/2019JD030857

Received 19 APR 2019
Accepted 5 OCT 2019
Accepted article online 23 OCT 2019
Published online 21 NOV 2019

Author Contributions:
Conceptualization: Jiaxi Hu, Daniel Rosenfeld
Data curation: Jiaxi Hu, Pengfei Zhang, Richard Weitz
Formal analysis: Jiaxi Hu, Daniel Rosenfeld, Alexander Ryzhkov
Funding acquisition: Alexander Ryzhkov, Dusan Zrnic
Investigation: Jiaxi Hu
Methodology: Jiaxi Hu, Daniel Rosenfeld
Project administration: Jiaxi Hu
Resources: Jiaxi Hu
Software: Jiaxi Hu
Supervision: Jiaxi Hu, Daniel Rosenfeld, Dusan Zrnic
Validation: Jiaxi Hu
Visualization: Jiaxi Hu
Writing - original draft: Jiaxi Hu
Writing – review & editing: Jiaxi Hu, Daniel Rosenfeld, Alexander Ryzhkov, *(continued)*

©2019. American Geophysical Union. All Rights Reserved.

1. Introduction

Until now, only global statistics have been presented to qualitatively address the relationships between aerosols, convective available potential energy (CAPE), and lightning. Aerosols can have profound impacts on cloud microphysics, precipitation formation, and cloud electrification. A larger concentration of cloud condensation nuclei (CCN) nucleate more numerous and smaller cloud droplets that are slower to coalesce into raindrops (Gunn & Phillips, 1957). On the other hand, cloud water that was not converted to rain is lifted to above the 0 °C level to become supercooled water or ice hydrometeors. The phase change from liquid to solid releases latent heat of freezing that invigorates convection and intensifies the precipitation (Rosenfeld et al., 2008). The cloud electrification is enhanced by a stronger mixed-phase process (Latham, 1981) that promotes charge separation between oppositely charged graupels and ice crystals within supercooled water clouds with strong updrafts (Reynolds et al., 1957; Takahashi, 1978; Williams, 1988). Therefore, the role of activated CCN

Dusan Zrnic, Earle Williams, Jeffrey C. Snyder, Renyi Zhang

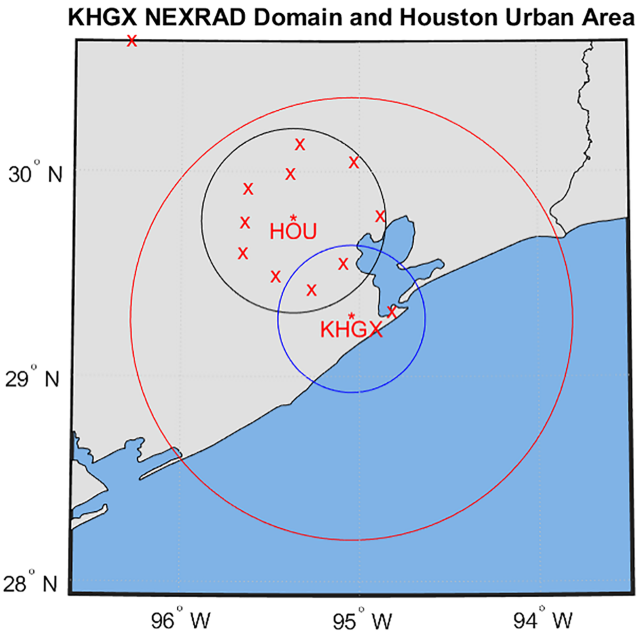

Figure 1. The domain of this study. KHGX represents the location of Houston/Galveston radar. The red crosses represent the 12 Houston LMA receivers used in this study. Also shown are the range circles of 40 (blue circle) and 120 km (red circle) from the radar, which were the lower and upper bounds for selecting the tracked cells. The Houston urban area is shown by the black circle within 50 km of the radar.

(N_{CCN}) in enhancing mixed-phase processes and updrafts was also proposed to enhance cloud electrification (Rosenfeld & Lensky, 1998; Williams et al., 2002). Further support for the role of aerosols in cloud invigoration and electrification has been provided by a number of other studies (Altaratz et al., 2014; Andreae et al., 2004; Fuchs et al., 2015; Ilotoviz et al., 2018; Khain et al., 2005; Khain et al., 2008; Mansell & Ziegler, 2013; Rosenfeld et al., 2008; Rosenfeld et al., 2014; Tao et al., 2007; Tao et al., 2012; van den Heever et al., 2006; van den Heever et al., 2011; Wang et al., 2011; Wang et al., 2014; Yuan et al., 2011), while other studies supported the role of CAPE (Bang & Zipser, 2016; Blanchard, 1998; Emanuel, 1997; Williams et al. 2002; Williams & Satori, 2004; Williams et al., 1992). A recent study showed strong evidence that increased aerosol in a remote marine environment resulting from ship emissions can more than double the amount of lightning over the shipping lanes compared to the background for the same CAPE (Thornton et al., 2017). An extensive study of convective features based on the Tropical Rainfall Measuring Mission showed an equal weight for CAPE and aerosol optical depth (Stolz et al., 2015; Stolz et al., 2017) on cloud electrification processes using a global database.

The purpose of this study is to examine individual convective cells and the way that CAPE and N_{CCN} affect the time-height evolution of dynamics, hydrometeors, and the resulting electrification within the convective clouds and storms. This is being done while controlling the differences in thermodynamic conditions, land/ocean contrast, and urban/rural area. Data used in this study include a composite from a nearby Next-Generation Radar (NEXRAD), the Suomi NPP satellite, a Lightning Mapping Array (LMA), and reanalysis soundings around the Houston region, which allows accurate convective cloud sampling and selection to understand aerosol effect under various conditions.

Here we examine the impact of an aerosol perturbation incurred by Houston (Figure 1) on the observed N_{CCN}, cloud microstructure, the evolution of hydrometeors, and cloud electrification by using a novel suite of tools developed for this objective. Houston is selected because it is a major source of anthropogenic aerosols on a relatively clean background in a climatic regime of deep moist convective clouds during summer. Houston and the surrounding vicinity are covered well by a polarimetric NEXRAD radar and an LMA (Figure 1). Houston is a major metropolis (population ~2.2 million) with an extensive petroleum industry; Houston hosts 14% of the refinery capacity of the United States (Corporation, 2018). Houston, located by the Texas Gulf coast, experiences various conditions that include oceanic clean, continental pristine, and continental polluted air masses. These conditions are well presented within the coverage of a single NEXRAD radar (KHGX Houston/Galveston radar site) and the Houston LMA. The Multi-Cell Identification and Tracking (MCIT) algorithm (Hu et al., 2019) package is used in this study as an automatic tool to identify and track convective precipitation cells from their first radar echo until their loss of identity during their dissipation. The MCIT provides the cells' life cycle properties including polarimetric quantities (from NEXRAD data), lightning information (i.e., LMA source count), and thermodynamic data (from sounding data). Here we quantify the influence of satellite-retrieved N_{CCN} (Rosenfeld et al., 2016) on the morphology, microphysical evolution, and electrification of ordinary convective storms. Each cloud cell is ascribed with relevant so-called "explaining" and "dependent" parameters from the aforementioned data sources. The explaining parameters include cloud-based activated CCN concentrations (hereafter, simply referred to as N_{CCN}), supersaturation (SS), surface-based CAPE (hereafter, simply referred to as CAPE), cloud base height (CBH), and two location descriptions (one of Land/Coastal/Ocean and one of Urban/Rural). The dependent parameters include reflectivity (Z), differential reflectivity (Z_{DR}), LMA source count, and additional parameters, as explained in the methodology part. It is worth noted that all explaining and dependent parameters patterns tested in this study is under the assumption that variability in other environment factors are not serving as alternative explanations.

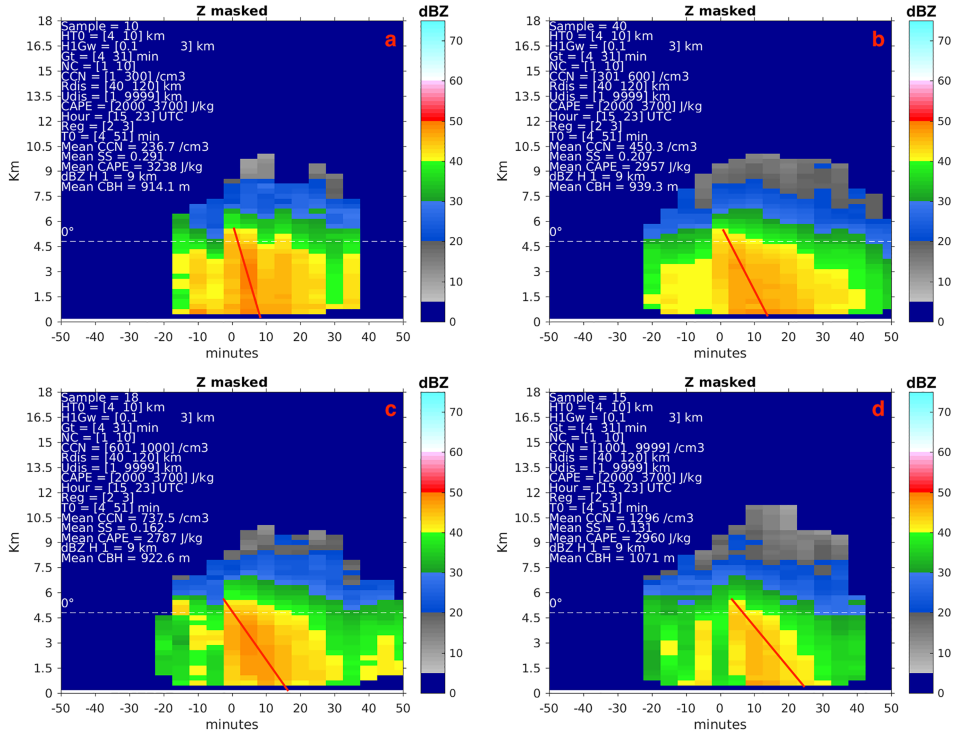

Figure 2. Time-height reflectivity composites of tracked cells. Time zero is defined as the time of first peak height of Z_{DR} > 1.5 dB. The composites are for N_{CCN} in four intervals: (a) 1–300 cm^3, (b) 301–600 cm^3, (c) 601–1,000 cm^3, and (d) >1,001 cm^3. The sample clouds include clouds from land only. The first detected echo top height is limited to be less than 9 km in order to filter out cells that were not tracked from their initiation. To isolate the microphysical effect of N_{CCN} from the invigoration feedback, the cloud vertical growth rate is limited to 3 km within the first 30 min. Detailed criteria are given in Table S2, sub 1.

2. Materials and Methods

The MCIT algorithm package (Hu et al., 2019) has been used as the primary tool to produce a data set with cloud cell lifetime information used in this study. A cell is defined as a local maximum in a vertically integrated liquid (VIL), where VIL is calculated with a fixed Z-R relationship from the WDSS II software package (Lakshmanan et al., 2007). The cells are tracked by the maximum common VIL in consecutive radar scans. Various parameters are collected for each cell. For instance, in this study, we use maximum Z and the corresponding Z_{DR} at each step of tracking at all elevation angles to construct time-height evolutions of the cloud cell life cycle. Polarimetric variable description can be found in our previous paper (Hu et al., 2019). To isolate the effect of N_{CCN} on the tracked cells' properties, each tracked cell was assigned to a class of N_{CCN}, while constraining the echo top height vertical growth rates within bounds of up to 3 km within the first 30 min (Figures 2 and 3). The integrated LMA source counts for each cell at each step of tracking at all elevations are also presented in section 3 under different cell selection criteria.

The N_{CCN} and supersaturation (SS) are retrieved from the Visible Infrared Imaging Radiometer Suite (VIIRS) onboard the Suomi National Polar-Orbiting Partnership (NPP) satellite by using convective clouds as natural CCN chambers (Rosenfeld et al., 2016). The activated CCN number concentration is equal to the satellite-retrieved cloud base drop concentration, which is calculated by a VIIRS-retrieved T-r_e relationship and cloud base updraft (W_b). Although the satellite only has one overpass (around 13:30 local time), we apply the retrieved N_{CCN} for ±3 hr. This time window is short with respect to the time scale of changes in air masses, while still allowing for a useful sample size. The N_{CCN}, SS, CBH, and W_b are retrieved from satellite data and mapped into the data records of the tracked cells by MCIT.

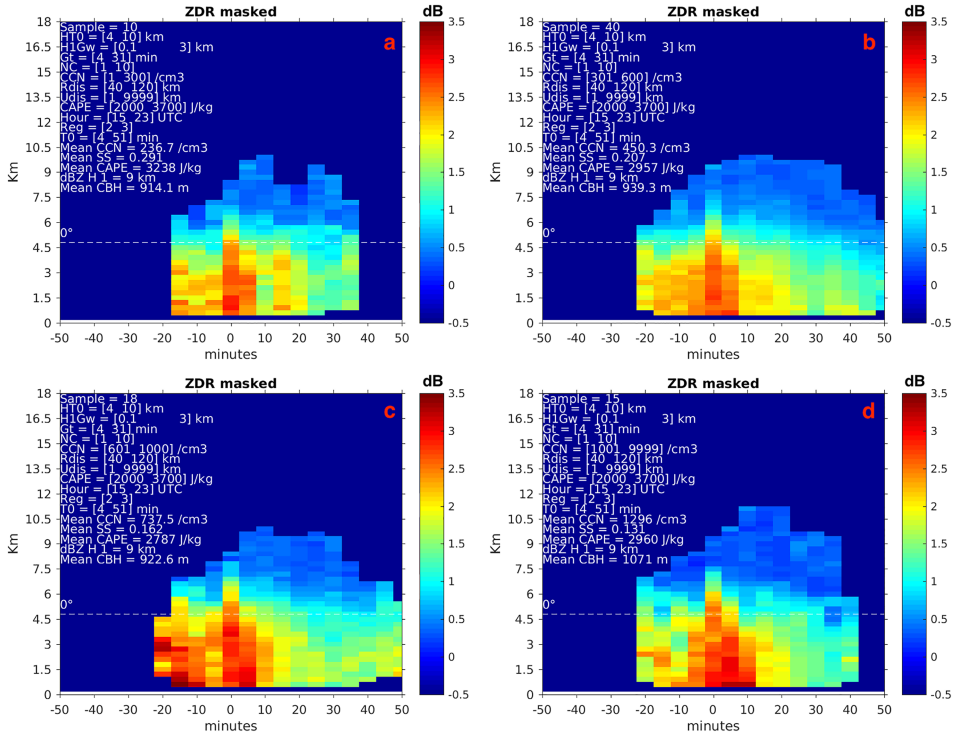

Figure 3. Same as in Figure 2 except for Z_{DR}. Detailed criteria are in Table S2, sub 1.

Cells were tracked under various conditions of CAPE and N_{CCN} and were further classified as occurring over land, coast, or ocean and as occurring over rural or urban areas. CAPE is retrieved from Eta Data Assimilation System (Project, 2004) with a temporal resolution of 3 hr and spatial resolution of 40 km. Events occurring during and around 19 satellite overpasses were analyzed, resulting in a total of 2,859 tracked cells. The cases are listed in Table S1 in the supporting information.

It is crucial to define selection criteria to divide cloud cell samples into different categories based on their various N_{CCN}, CAPE, and regional attributes in order to compare the effect these attributes have on hydrometeor and lightning properties. A complete table of selection criteria can be found in Table S3. Here we discuss a few important criteria. To isolate the microphysical from thermodynamic effects, the initial (within the first 30 min) growth rate of each cell's echo top height is restricted to be less than 10 m/s. The analyses are done with and without this restriction.

In this study, echo top height for each cell is defined as the highest reflectivity that exceeds 0 dBZ.

The cells that pass the selection criteria are composited by averaging them after shifting their times to a common time basis. Pixels that are contributed by less than 50% of selected samples for each scenario are masked. After masking, each pixel in the composite time-height coordinate represents the average value contributed by the selected cells at that time step and height. For instance, 100 cells are selected to construct a composite figure with different height range and lifetime duration. Pixels with contributions from less than 50 cells will be masked. The individual values for pixels with contribution from over 50 cells are averaged. Two different reference times (t0) are used to create two sets of composites—one based on radar data and one based on lightning data. To study the N_{CCN} effect on cloud microstructure and invigoration, t_0 was defined as the time step where $Z_{DR} > 1.5$ dB reached a peak height for the first time. This is the time when the largest raindrops in the updraft start to fall or freeze. Indeed, the composites in Figure 3 clearly show patterns of rain shafts initiated aloft at t_0. Superposition of the cells' lightning properties was done by defining the time of first lightning as t_0. This allows assessing the time evolution of lightning as a function of different N_{CCN}, CAPE, and location/region. Cells that had no LMA-detected lightning sources were not included. Z_{DR} t0 and lightning t0 are two separate terms and do not affect each other.

3. Results

3.1. N_{CCN} Effect on Cloud Microphysics

First, we test the role of N_{CCN} on the hydrometeors of convective cells while excluding the aerosol invigoration effect. This is done by selecting cells that have initial vertical growth rates (as seen in their echo top heights) less than 10 m/s. The idea to limit selected cases growth rate in Figures 2–4 is to choose cells that were tracked well within their growing stage, as opposed to some cells that appeared later in their life cycle as a result of merging or splitting. The cloud top rising rate is typically half of the cloud updraft due to the divergence and mixing near cloud top. Therefore, this criterion practically limits the growing stage to cells with updrafts <~20 m/s. This includes most of cells during their growing stage while excluding cells that are not tracked in their growing stage. The criterion of selecting cells with a growth rate less than 10 m/s is empirical and optimized by the size of this data set. The full classification criteria are shown in Table S2. The t_0 for superpositioning of the cells is set to the time of large raindrops start to fall.

Figure 2 shows the time-height evolution of the reflectivity patterns for four intervals of N_{CCN} (less than 300, 301–600, 601–1,000, and greater than 1,000 CCN/cm^3), in Figures 2a–2d, respectively. CAPE is limited between 2,000 and 3,700 J/kg so that the cloud samples in each N_{CCN} interval have similar mean CAPE values. The respective CAPE histograms are shown in Figure S15. The similarity in CAPE reduces the probability that differences observed are attributable to differences in CAPE. The weight linear regression fit is calculated by using Matlab function "robustfit." The input correlation parameters are height and time. It is operated on a time window within the tracked cell, from the initial time of tracking to the end of first Z_{DR} shaft (collapse of first Z_{DR} column), as identified by a minimum in the low level Z_{DR}. The bi-square weighting function parameters are reflectivity for rain shaft and Z_{DR} for Z_{DR} shaft calculations. The slope for each cell's shafts is created by using the fitted linear slope and axis intercept output from the Matlab robustfit function. The averaged line in Figure 2 is created by using averaged slopes and intercept values from all the cells that are incorporated in the cell composition. The descending maxima of Z that are evident in Figure 2 indicate the descending cores of the first precipitation shafts. The core reaches the ground ~10 min after its initiation aloft for average N_{CCN} < 300 cm^3 (Figure 2a) but increases to ~20 min for the N_{CCN} > 1,000 cm^3. This increase in the time that it takes the precipitation core to reach the ground has high statistical significance (Figure 2c and Table S4, sub 1). These patterns behave according to expectations that large concentrations of CCN inhibit coalescence and delay the initiation of major rain shaft. The initial location of cell samples can be found in Figure S1.

Figure 3 shows the time-height evolution of Z_{DR} using the same cloud samples and N_{CCN} intervals as in Figure 2. The core of peak Z_{DR} reaches the ground some 5 to 15 min before the reflectivity cores do, with significant longer time for the higher N_{CCN} cases (Figure 4b and Table S4, sub 2). This indicates that the initial, relatively sparse large raindrops that form in the clouds fall before the main precipitation shaft owing to their larger fall speeds.

Box plots of the evolution of the main precipitation shaft (time to reach the ground) and the Z_{DR} shaft are shown in Figures 4a and 4b, respectively. The Z and Z_{DR} shafts are calculated by weighted linear regression function (Pozo, 1997), and the amount of time that they take to reach the ground is the intercept to the x axis calculated from the regression function. These box plots use the same samples and N_{CCN} intervals as shown in Figures 2 and 3. Individual cell's rain shaft and Z_{DR} shaft are calculated in each N_{CCN} interval for the statistics shown in Figure 4. The mean amounts of time for the Z shaft to reach the ground, marked by the red lines, for the four CCN intervals are 14.5, 20, 23.3, and 29.7 min, respectively. The mean times for the Z_{DR} shaft to reach the ground for the four N_{CCN} intervals are 9, 13.7, 15, and 22 min, respectively. These results support the pattern of delayed rain initiation and are consistent with the patterns seen in Figure 2.

The median volume diameter (D_0) of raindrops is retrieved by equation (1) (Bringi & Chandrasekar, 2001):

$$D_0(mm) = 1.53[Z_{DR}(dB)]^{0.47} \quad (1)$$

The magnitude of D_0 increases with increasing N_{CCN}, indicating larger hydrometeors with more CCN (Figure S2). This is ascribed to the CCN-induced suppressed coalescence, which leaves more cloud water

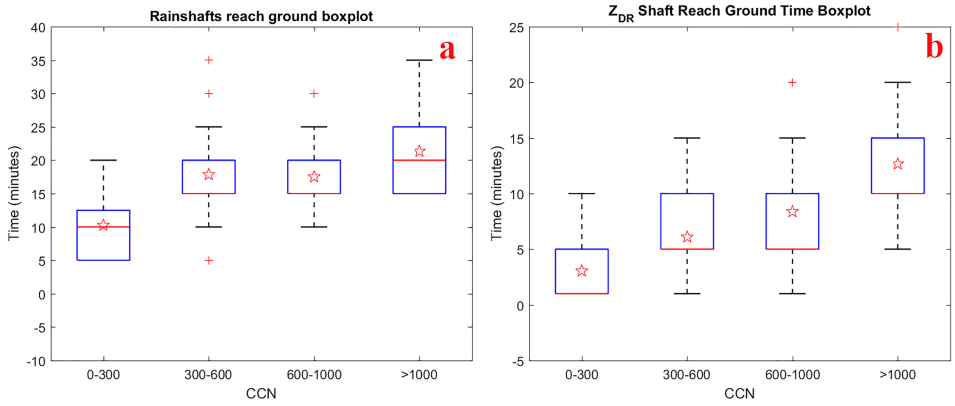

Figure 4. Box plots of the time difference from rainshaft initiation aloft until they reach ground (Figure 3a) and the same for Z_{DR} shafts, for the same N_{CCN} interval as Figures 2 and 3. Rainshaft and ZDR shaft are calculated with a weighted linear regression function (Pozo, 1997) between height and maximum Z or Z_{DR} in the vertical. The stars represent the mean values. Detailed criteria are in Table S2, sub 1.

available for faster accretion and resultant growth of raindrops or hailstones. (The statistical significance of the dependence of D_0 on N_{CCN} is shown in Figure S3.)

Figure 5 shows the N_{CCN} convection invigoration effect on the maximum echo top heights (H_{max}; km). The box plots of H_{max} in Figure 5 are made for the same N_{CCN} intervals as in Figures 2 and 3. Therefore, CAPE values for the N_{CCN} groups are also similar. The mean values of H_{max} increase with N_{CCN} from 10.5 km ($N_{CCN} < 300$ cm^3) to 12.9 km (600–1,000 cm^3) and become steady (or "saturated") for higher N_{CCN}. The indicated increase in H_{max} is statistically significant (Table S4, sub 3) and serves as a manifestation of the aerosol invigoration effect. The initial location of cell samples can be found in Figure S4.

3.2. N_{CCN} Effect on Lightning

To study the N_{CCN} effect on lightning, we first select convective cells that have detected LMA sources. The cells are composited with t_0 defined as the time of detection of the first LMA source. Figure 6 shows the time-height composition of the LMA source count for four N_{CCN} concentration intervals of less than 400, 400–800, 800–1,200, and greater than 1,200 cm^3, as shown in Figures 6a–6d, respectively. The N_{CCN} intervals in Figure 6 are different than those in Figures 2–5 because there is a scarcity of cells with lightning at low N_{CCN} concentrations. CAPE is limited to between 2,000 and 4,000 J/kg in order to keep all N_{CCN} scenarios within similar thermodynamic conditions. According to Figures 6a–6d, LMA source count increases with increasing N_{CCN} concentration to an optimal range of 800–1,200 cm^3 (the average within this range is 955 cm^3) and decreases when the N_{CCN} concentration exceeds 1,200 cm^3; additional significant results can be found in Figure S7 and Table S3, sub 4. The enhanced lightning activity that is seen in Figures 6a–6c is likely due to the delayed warm rain process associated with higher N_{CCN}, which allows cloud drops to reach higher altitudes, enhancing mixed-phase processes and resulting in stronger updrafts (Rosenfeld et al., 2008). This creates favorable conditions for charge separation as nonneutral charge buildup occurs as hail/graupel collide with ice crystals in a supercooled cloud that has a strong updraft. There is a limit, however, where increasing N_{CCN} becomes associated with decreasing lightning activity as seen in the highest N_{CCN} (Figure 6d; mean N_{CCN} = 1,354 cm^3). According to previous observations in China (Rosenfeld et al., 2011) and Isreal-India (Braga et al., 2017), high N_{CCN} of smaller drops reduce the probability of freezing by limiting hydrometeor contact possibilities and do not support secondary ice

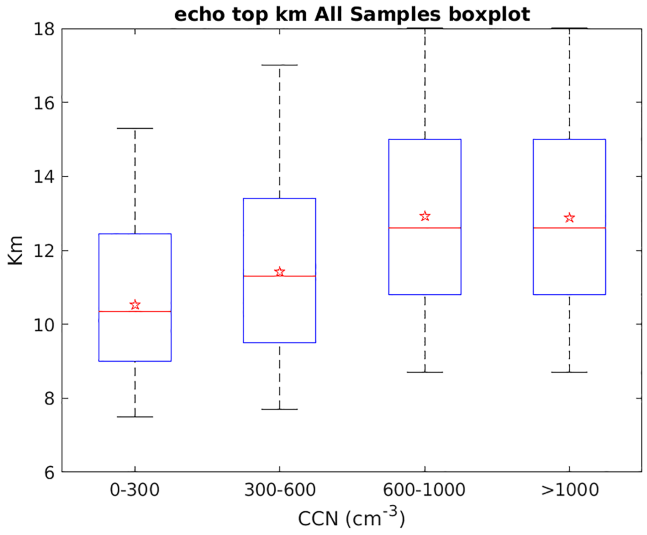

Figure 5. Box plots of max echo top height (km) of cloud samples using the same N_{CCN} interval as Figures 2 and 3. The first growth height and time limitations as in Figures 2 and 3 are released in order to show the N_{CCN} invigoration effect. Other criteria stay the same as Figures 2 and 3. Detailed criteria are given in Table S2, sub 2.

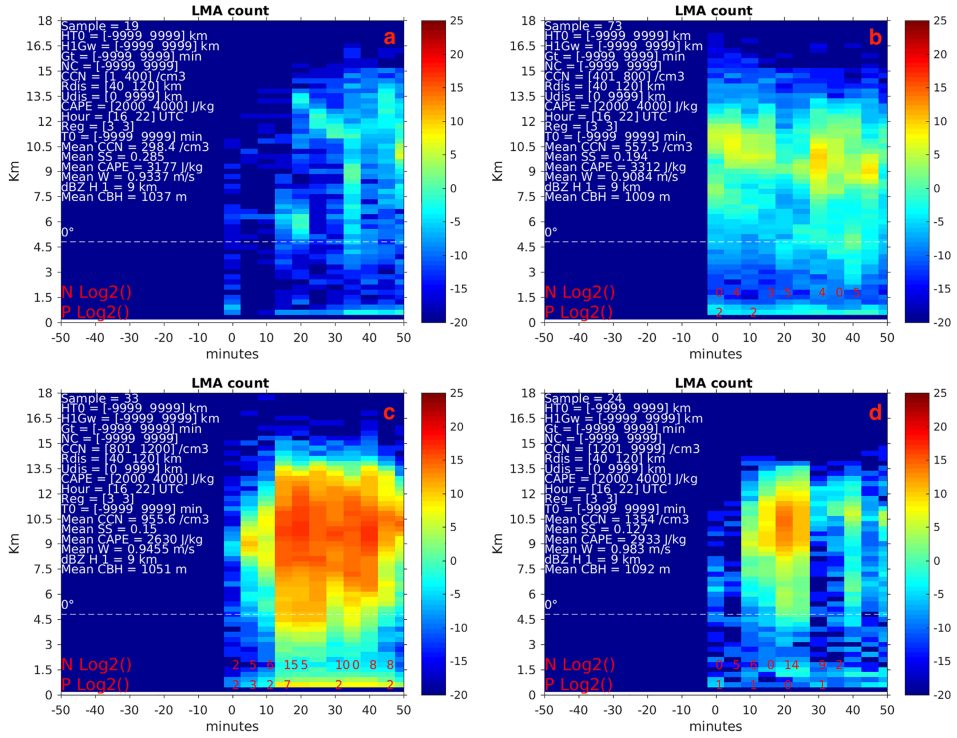

Figure 6. Composite time-height evolution LMA source count in radar tracked convective cells under different N_{CCN}. The color scale is ($10*\log_{10}$ (N)), where N is the number of LMA sources per 5 min with a vertical resolution of 300 m. The composites are shown for N_{CCN} of (a) <400 cm^3, (b) 400–800 cm^3, (c) 800–1,200 cm^3, and (d) >1,200 cm^3. The growth-related criteria are released in all the figures of LMA source counts. CAPE is constrained between 2,000 and 4,000 J/kg. The rest criteria are identical as Figures 2 and 3. Detailed criteria are given in Table S2, sub 3.

formation. With N_{CCN} exceeding optimal range (N_{CCN} >1,200 cm^3 in this study), the initiation of ice crystals is delayed until higher altitudes (Braga et al., 2017; Rosenfeld et al., 2011). Since the top of the mixed-phase layer cannot exceed the height of the −38 °C isotherm, delayed ice crystal initiation decreases the depth of the layer where robust cloud electrification can take place. The initial location of cell samples can be found in Figure S8.

The ambiguity between the roles of N_{CCN} and CAPE (i.e., the thermodynamic impact) on lightning occurrence was addressed in this study by classifying the tracked cells into low and high N_{CCN} groups occurring in low and high CAPE environments, which allows us to better separate the role that N_{CCN} and CAPE have on lightning occurrence. Convective inhibition (CIN) versus CAPE scatterplot is shown in Figure S20. The overall inversion is weak (CIN > −100 J/kg) with only 50 out of 2,859 cells' CIN less than −100 J/kg for CAPE less than 1,000 J/kg. Figure 7 shows time-height composites of the LMA source counts under different N_{CCN} and CAPE combinations. On the left-hand side (LHS) of Figure 7 (Figures 7a and 7c), the CAPE values of sample convective cells are limited to less than 3,000 J/kg with either low N_{CCN} (i.e., less than 500 cm^3; Figure 7a) or high N_{CCN} (i.e., greater than 500 cm^3; Figure 7c) concentrations. The right-hand side (RHS) of Figure 7 (Figures 7b and 7d) has the same N_{CCN} partition but is valid for cells occurring in environments of CAPE >3,000 J/kg. By comparing the LHS and RHS of Figure 7 (Figure 7a versus 7c or Figure 7b versus 7d) vertically, the enhanced lightning associated with increasing N_{CCN} concentration (mean N_{CCN} increases from 360 to 924 cm^3 from Figures 7a–7c for example) is apparent, although it should be noted that mean CAPE decreased slightly from 2,604 J/kg (Figure 7a) to 2,376 J/kg. These observations support the idea that increasing N_{CCN} enhances mixed-phase precipitation and affects lightning as previously discussed.

On the other hand, comparing Figure 7 panels horizontally (i.e., Figure 7a versus 7b or Figure 7c versus 7d) elucidates the CAPE effect on lightning. For instance, Figures 7a and 7b have similar mean N_{CCN} (360 cm^3 for Figure 7a and 373 cm^3 for Figure 7b), but Figure 7b has about 1,000 J/kg higher mean CAPE. The

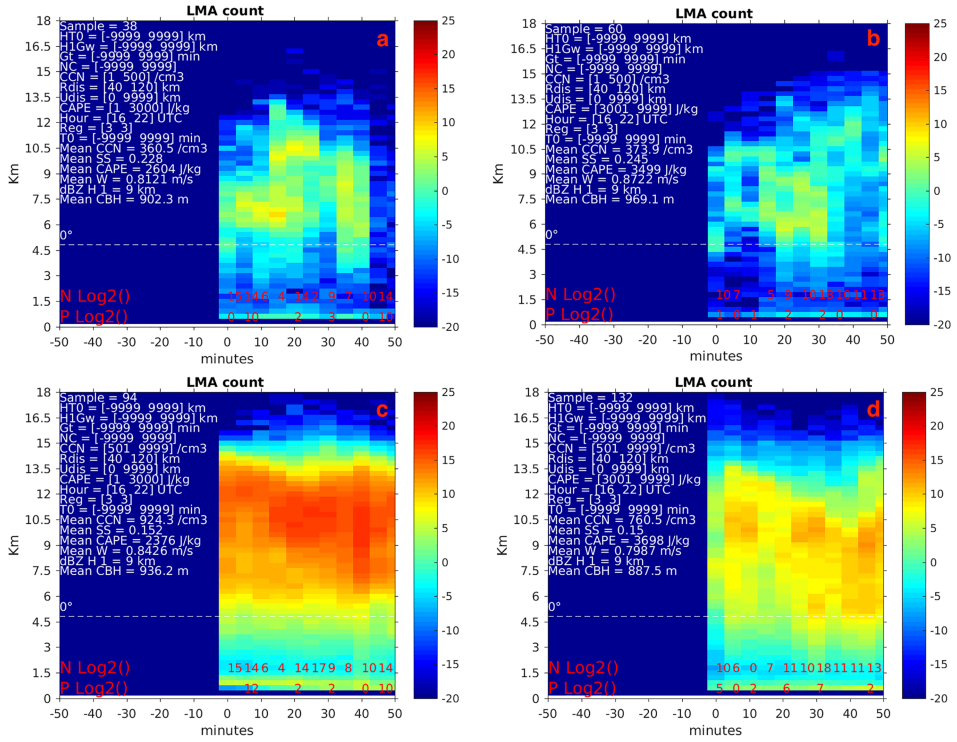

Figure 7. Same as Figure 6 but for combined classification of CAPE and N_{CCN}. The N_{CCN} classes are (a and b) <500 cm^3 and (c and d) >500 cm^3. The CAPE classes are (a and c) 1,500–3,000 J/kg and (b and d) >3,000 J/kg. The CAPE starts with 1,500 J/kg for the sample clouds due to the lack of samples with lightning associated with CAPE <1,500 J/kg. The remaining criteria are as in Figure 6. Detailed criteria are given in Table S2, sub 4.

lightning enhancement is not obvious with higher CAPE when keeping the N_{CCN} similar; the evidence that higher CAPE enhances mixed phase process and the resultant charge separation and lightning is not seen in these data. However, Figures 7c and 7d did not show such lightning enhancement for the high N_{CCN}. Although Figure 7d samples have a much higher mean CAPE (3,698 J/kg) than Figure 7c (2,197 J/kg), the lightning is not enhanced, and it even decreased to some extent. This result suggests that CAPE is not important to enhancing lightning, at least in the sample of cells examined herein. Once CAPE is sufficient to support deep convective clouds, N_{CCN} appears to dominate the lightning activity, and these results are statistically significant, as shown in Table S3, sub 5. The initial location of cell samples can be found in Figure S10.

Another outstanding question is the ambiguity between the impacts of urban aerosol emissions and urban heat island effect on lightning. Previous studies (Bourscheidt et al., 2016; Orville et al., 2001; Soriano & de Pablo, 2002; Stallins, 2004) have pointed out that urban areas tend to enhance lightning with respect to nearby rural areas because urban areas generally have, among other differences, higher CAPE, more N_{CCN}, and more complicated surface roughness conditions. In this study, an urban area is defined as a 50-km radius circle centered at Houston city center (29.7604°N, 95.3698°W). The rural area includes the rest of the search domain centered at KHGX (Houston/Galveston, TX radar) radar site (Figure 1). The cloud cells over the Gulf of Mexico have been excluded for this selection because of possible additional difference between land and sea surface properties.

The time-height evolutions of LMA source counts in rural and urban areas are compared in Figure 8. The LHS panels of Figure 8 show the lightning in the rural area with low (Figure 8a; N_{CCN} <500 cm^3) and high (Figure 8c; N_{CCN} >500 cm^3) N_{CCN}. The RHS panels show the lightning source counts in the urban area with the same N_{CCN} classes. By comparing the panels vertically (i.e., Figure 8a versus 8c and Figure 8b versus 8d), increasing N_{CCN} concentration induced significantly more numerous lightning sources as expected from the previous discussion both in the rural and urban areas. On the other hand, comparing panels horizontally

(Figure 8a versus 8b and Figure 8c versus 8d) indicates that urban area has significantly more lightning than the rural area under similar N_{CCN} and CAPE conditions primarily when N_{CCN} was low. The increase of number of lightning events from selected cells is small and statistically insignificant under high N_{CCN} (the significance levels can be found in Table S4, sub 6). The lightning enhancement over urban areas has been previously attributed to the urban topography (Bornstein et al., 1990) and to the urban heat island effect (Pinto, 2013). The urban heat island effect is characterized by locally higher temperatures, with little or no change in absolute humidity, thus increasing cloud base heights (owing to lower mean relative humidity) and updraft strength (owing to higher temperatures). This hypothesis can be tested by comparing the cloud base heights in the urban and rural areas (Figure S12). The cloud base heights between rural and urban areas under similar N_{CCN} and thermodynamic conditions are similar and show no statistically significant differences, which means that the urban heat island probably does not play a significant role here. Note that, since the urban heat island effect impacts CAPE, we reduce some of the impact of the urban heat island by grouping the data by similar CAPE. The initial location of cell samples can be found in Figure S13.

Low N_{CCN} over the Houston urban area are possible despite the large emission source because most of the newly formed aerosols there are ultrafine aerosol particles (UAPs) that are too small to serve as CCN (Almeida et al., 2016; Pikridas et al., 2015). However, it was recently shown that UAP can invigorate deep tropical convective clouds with low N_{CCN} (Fan et al., 2018; Khain et al., 2012). The low N_{CCN} leads to fast coalescence that reduces the integrated drop surface area and increases the vapor supersaturation (S) to more than 10% in the absence of large numbers of UAP. The added UAP (of urban origin in this case) can activate additional cloud droplets at an S of a few percent, which limits S to lower values. This results in additional production of cloud droplets aloft along with condensation and respective latent heat release that invigorate the convection and enhance the lightning. This could be a major contributor to lightning enhancement by aerosol and should draw attention to future studies.

Previous studies indicated that CBH and wind shear are important parameters in regulating lightning activities (Stolz et al., 2017; Williams et al., 2005). In this study, CBH is used as a control parameter in each above scenario (Figures 2–8) to assure that all panels have similar CBH conditions. The mean CBH values for each classification can be found in Table S2. Fan et al. (2009) showed that wind shear >10 m/s suppresses the invigoration. The wind shear is calculated as a vector difference between 925- and 500-hPa winds and is hereafter referred to as SHEAR. The SHEAR distributions are shown in Figures S4, S6, S9, S11, and S14. The median values of SHEAR for the various classifications (Table S6) are generally less than 5 m/s and are considered in the weak SHEAR category. Therefore, SHEAR has little effect on the overall conclusions in this study. CBH, SHEAR, and other thermodynamic parameters do affect lightning activity and polarity, but environments other than Houston provide a much larger range of these properties. The relatively small dynamic range in these variables in this study provides the benefit of allowing us to focus on the effect of N_{CCN}.

4. Conclusions

The Houston area serves as a natural laboratory for identifying and examining the effects of aerosols on cloud microstructure, precipitation-forming processes, and cloud electrification. The setting of abundant deep moist precipitating clouds occurring over a major metropolis with many industrial emission sources on the shore of a tropical ocean with onshore flow allows one to examine the differences between polluted and clean clouds over land and to study the large variability of aerosols from marine, rural, and urban origins. A unique combination of polarimetric radar, LMA, and newly developed satellite retrievals of N_{CCN} makes it possible, for the first time, to evaluate quantitatively the observed effects of N_{CCN} on cloud microphysical, dynamic, and electrification properties. The main results show that

1. Increased N_{CCN} delays the initiation of precipitation (Figures 2–4). The physics behind this is that more CCN leads to more numerous and smaller cloud droplets and weakened coalescence, which delays the initiation of warm rain.
2. Increased N_{CCN} invigorate the convection as indicated by increased H_{max}. The effect saturates near N_{CCN} = 1,000 cm^3, as shown in Figure 5. Since N_{CCN} is decorrelated from CAPE in the study area, these observations are in line with the aerosol convective invigoration hypothesis (Rosenfeld et al., 2008).

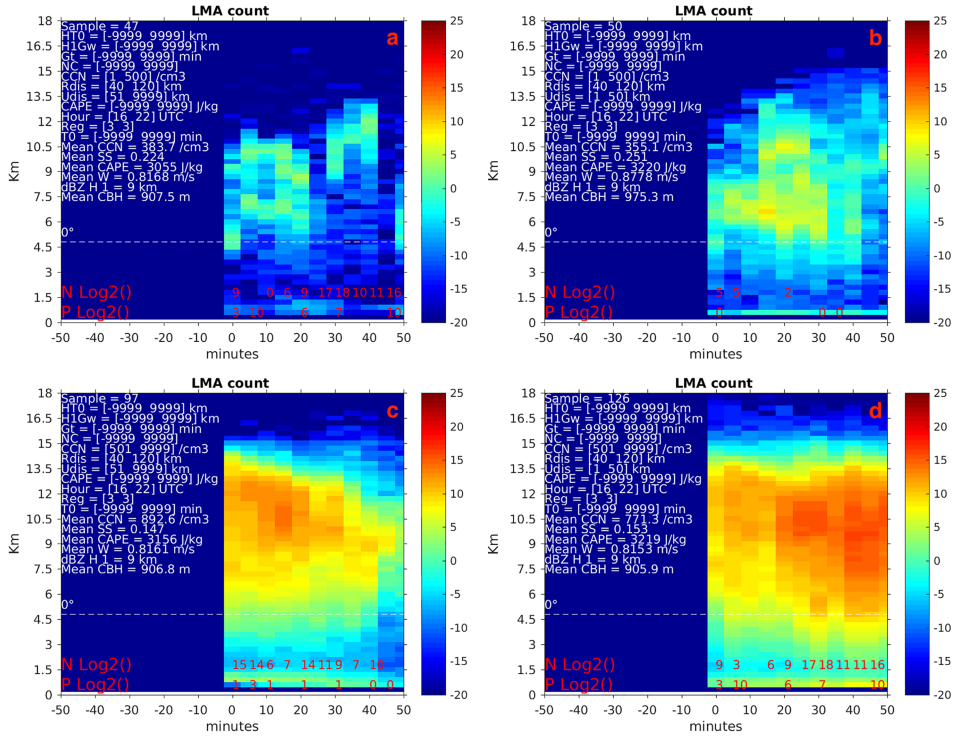

Figure 8. Same as Figure 7 but for urban and land rural areas under low and high N_{CCN}. (a and b) N_{CCN} <500 cm^3 and (c and d) N_{CCN} >500 cm^3. (a) and (c) are over rural areas, whereas (b) and (d) are over urban areas. Detailed criteria are given in Table S2, sub 5.

3. Increasing N_{CCN} from <400 cm^3 to the range of 800–1,200 cm^3 is associated with an increase of lightning activity by 1 order of magnitude when holding CAPE constant (Figures 6a–6c). This is in line with the aerosol convective invigoration effect which brings more cloud water and larger updrafts to the temperature range where mixed phase precipitation and cloud electrification can occur.
4. Increasing N_{CCN} further beyond 1,200 cm^3 has the opposite effect, that is, reducing lightning activity (Figures 6c and 6d). It is hypothesized that this is caused by the increasing height of ice initiation when supercooled cloud droplets are smaller.
5. Adding CAPE in moderate to high CCN environment (e.g., N_{CCN} >500 cm^3) does not further enhance the (already high) lightning activity (Figures 7c and 7d). The enhanced updrafts probably push the cloud electrification beyond the optimal point by delaying the initiation of mixed-phase processes to higher altitudes.
6. In a low N_{CCN} environment (N_{CCN} <500 cm^3), the urban area has considerably more lightning than does the rural area, but the effect fades at higher N_{CCN} (Figure 8). There is no indication of an urban heat island effect on cloud base heights. It is hypothesized that the urban ultrafine aerosols that are too small to serve as CCN at cloud base are activated into additional cloud droplets aloft and invigorate the convection by additional latent heating during the added condensation and freezing. This mechanism can also add or increase supercooled water and further enhance the cloud electrification.

CAPE is essential for the initiation of deep convection. When CAPE is sufficient for deep moist convection, aerosol concentration can strongly affect the lightning activity. The low magnitude of the wind shear for the cases in this study reduces the probability that changes in wind shear are responsible for the observed differences in precipitation and lightning characteristics. The aerosols include both activated CCN and smaller particles, which may activate cloud droplets and invigorate the convection well above cloud base. This study serves as an impetus for additional in situ observations of aerosols, microphysical characteristics, and thermodynamic properties in the Houston area (and in other geographical domains) in order to better test and substantiate the hypotheses and conclusions of this study.

Acknowledgments

Funding was provided by NOAA/Office of Oceanic and Atmospheric Research under NOAA-University of Oklahoma cooperative agreement NA11OAR4320072, U.S. Department of Commerce, and by the U.S. National Weather Service, Federal Aviation Administration, and Department of Defense program for modernization of NEXRAD radars. Additional funding came from Department of Energy grants DE-SC0014295 and DE-SC0018967. Data used here are obtained from National Centers for Environmental Information (https://www.ncdc.noaa.gov/data-access). Tracking data set and code used in this study is archived in a NSSL ftp link (ftp://ftp.nssl.noaa.gov/users/pzhang/).

References

Almeida, G. P., Santana, M. E., Sousa, R., & Godoi, R. (2016). Aircraft observations of the interactions of the manaus plume with aerosols forest during rainy season: A case study. *Ciência e Natura*, *38*, 7.

Altaratz, O., Koren, I., Remer, L. A., & Hirsch, E. (2014). Review: Cloud invigoration by aerosols-Coupling between microphysics and dynamics. *Atmospheric Research*, *140*, 38–60.

Andreae, M. O., Rosenfeld, D., Artaxo, P., Costa, A. A., Frank, G. P., Longo, K. M., & Silva-Dias, M. A. F. (2004). Smoking rain clouds over the Amazon. *Science*, *303*(5662), 1337–1342. https://doi.org/10.1126/science.1092779

Bang, S. D., & Zipser, E. J. (2016). Seeking reasons for the differences in size spectra of electrified storms over land and ocean. *Journal of Geophysical Research: Atmospheres*, *121*, 9048–9068.

Blanchard, D. O. (1998). Assessing the vertical distribution of convective available potential energy. *Weather and Forecasting*, *13*, 870–877.

Bourscheidt, V., Pinto, O., & Naccarato, K. P. (2016). The effects of Sao Paulo urban heat island on lightning activity: Decadal analysis (1999-2009). *Journal of Geophysical Research: Atmospheres*, *121*, 4429–4442.

Braga, R. C., Rosenfeld, D., Weigel, R., Jurkat, T., Andreae, M. O., Wendisch, M., et al. (2017). Further evidence for CCN aerosol concentrations determining the height of warm rain and ice initiation in convective clouds over the Amazon basin. *Atmospheric Chemistry and Physics*, *17*, 14,433–14,456.

Bringi, V., & Chandrasekar, V. (2001). *Polarimetric Doppler Weather Radar: Principles and Applications*. Cambridge, England: Cambridge University Press.

Corporation, T. E. D. (2018). Petroleum Refining & Chemical Products. Retrieved from https://businessintexas.com/industries/petroleum-refining-chemical-products

Emanuel, K. A. (1997). Overview of atmospheric convection. *Nato Adv Sci I C-Mat*, *505*, 1–28.

Fan, J. W., Rosenfeld, D., Zhang, Y., Giangrande, S. E., Li, Z., Machado, L. A., et al. (2018). Substantial convection and precipitation enhancements by ultrafine aerosol particles. *Science*, *359*, 411.

Fan, J. W., Yuan, T., Comstock, J. M., Ghan, S., Khain, A., Leung, L. R., et al. (2009). Dominant role by vertical wind shear in regulating aerosol effects on deep convective clouds. *Journal of Geophysical Research*, *114*. D012352. https://doi.org/10.1029/2009JD012352

Fuchs, B. R., Rutledge, S. A., Bruning, E. C., Pierce, J. R., Kodros, J. K., Lang, T. J., et al. (2015). Environmental controls on storm intensity and charge structure in multiple regions of the continental United States. *Journal of Geophysical Research: Atmospheres*, *120*, 6575–6596.

Gunn, R., & Phillips, B. B. (1957). An Experimental Investigation of the Effect of Air Pollution on the Initiation of Rain. *Journal of Meteorology*, *14*, 272–280.

Hu, J., Rosenfeld, D., Zrnic, D., Williams, E., Zhang, P., Snyder, J. C., et al. (2019). Tracking and characterization of convective cells through their maturation into stratiform storm elements using polarimetric radar and lightning detection. *Atmospheric Research*.

Ilotoviz, E., Khain, A., Ryzhkov, A. V., & Snyder, J. C. (2018). Relationship between Aerosols, Hail Microphysics, and ZDR Columns. *Journal of the Atmospheric Sciences*, *75*, 1755–1781.

Khain, A., Rosenfeld, D., & Pokrovsky, A. (2005). Aerosol impact on the dynamics and microphysics of deep convective clouds. *Quarterly Journal of the Royal Meteorological Society*, *131*, 2639–2663.

Khain, A. P., BenMoshe, N., & Pokrovsky, A. (2008). Factors determining the impact of aerosols on surface precipitation from clouds: An attempt at classification. *Journal of the Atmospheric Sciences*, *65*, 1721–1748.

Khain, A. P., Phillips, V., Benmoshe, N., & Pokrovsky, A. (2012). The Role of Small Soluble Aerosols in the Microphysics of Deep Maritime Clouds. *Journal of the Atmospheric Sciences*, *69*, 2787–2807.

Lakshmanan, V., Smith, T., Stumpf, G., & Hondl, K. (2007). The Warning Decision Support System-Integrated Information. *Weather and Forecasting*, *22*, 596–612.

Latham, J. (1981). The Electrification of Thunderstorms. *Quarterly Journal of the Royal Meteorological Society*, *107*, 277–298.

Mansell, E. R., & Ziegler, C. L. (2013). Aerosol Effects on Simulated Storm Electrification and Precipitation in a Two-Moment Bulk Microphysics Model. *Journal of the Atmospheric Sciences*, *70*, 2032–2050.

Orville, R. E., Huffines, G., Nielsen-Gammon, J., Zhang, R., Ely, B., Steiger, S., et al. (2001). Enhancement of cloud-to-ground lightning over Houston, Texas. *Geophysical Research Letters*, *28*, 2597–2600.

Pikridas, M., Sciare, J., Freutel, F., Crumeyrolle, S., Von Der Weiden-Reinmüller, S. L., Borbon, A., et al. (2015). In situ formation and spatial variability of particle number concentration in a European megacity. *Atmospheric Chemistry and Physics*, *15*, 10,219–10,237.

Pinto, O. (2013). Lightning and climate: a review. *International Symposium on Lightning Protection (Xii Sipda)*, *2013*, 402–404.

Pozo, R. (1997). Template numerical toolkit for linear algebra: High performance programming with C++ and the standard template library. *The International Journal of Supercomputer Applications*, *11*, 251–263.

Project, N. C. G. C. 2004, cited 2018: NAM Data Assimilation System. [Available online at https://www.ready.noaa.gov/archives.php.]

Reynolds, S. E., Brook, M., & Gourley, M. F. (1957). Thunderstorm Charge Separation. *Journal of Meteorology*, *14*, 426–436.

Rosenfeld, D., Andreae, M. O., Asmi, A., Chin, M., de Leeuw, G., Donovan, D. P., et al. (2014). Global observations of aerosol-cloud-precipitation-climate interactions. *Reviews of Geophysics*, *52*, 750–808.

Rosenfeld, D., & Lensky, I. M. (1998). Satellite-based insights into precipitation formation processes in continental and maritime convective clouds. *Bulletin of the American Meteorological Society*, *79*, 2457–2476.

Rosenfeld, D., Lohmann, U., Raga, G. B., O'Dowd, C. D., Kulmala, M., Fuzzi, S., et al. (2008). Flood or drought: How do aerosols affect precipitation? *Science*, *321*(5894), 1309–1313. https://doi.org/10.1126/science.1160606

Rosenfeld, D., Yu, X., Liu, G., Xu, X., Zhu, Y., Yue, Z., et al. (2011). Glaciation temperatures of convective clouds ingesting desert dust, air pollution and smoke from forest fires. *Geophysical Research Letters*, *38*, L21804. https://doi.org/10.1029/2011GL049423

Rosenfeld, D., Zheng, Y., Hashimshoni, E., Pöhlker, M. L., Jefferson, A., Pöhlker, C., et al. (2016). Satellite retrieval of cloud condensation nuclei concentrations by using clouds as CCN chambers. *Proceedings of the National Academy of Sciences of the United States of America*, *113*, 5828–5834.

Soriano, L. R., & de Pablo, F. (2002). Effect of small urban areas in central Spain on the enhancement of cloud-to-ground lightning activity. *Atmospheric Environment*, *36*, 2809–2816.

Stallins, J. A. (2004). Characteristics of urban lightning hazards for Atlanta, Georgia. *Climatic Change*, *66*, 137–150.

Stolz, D. C., Rutledge, S. A., & Pierce, J. R. (2015). Simultaneous influences of thermodynamics and aerosols on deep convection and lightning in the tropics. *Journal of Geophysical Research: Atmospheres*, *120*, 6207–6231.

Stolz, D. C., Rutledge, S. A., Pierce, J. R., & van den Heever, S. C. (2017). A global lightning parameterization based on statistical relationships among environmental factors, aerosols, and convective clouds in the TRMM climatology. *Journal of Geophysical Research: Atmospheres*, *122*, 7461–7492.

Takahashi, T. (1978). Riming Electrification as a Charge Generation Mechanism in Thunderstorms. *Journal of the Atmospheric Sciences*, *35*, 1536–1548.

Tao, W. K., Chen, J. P., Li, Z. Q., Wang, C., & Zhang, C. D. (2012). Impact of Aerosols on Convective Clouds and Precipitation. *Reviews of Geophysics*, *50*RG2001. https://doi.org/10.1029/2011RG000369.

Tao, W. K., Li, X. W., Khain, A., Matsui, T., Lang, S., & Simpson, J. (2007). Role of atmospheric aerosol concentration on deep convective precipitation: Cloud-resolving model simulations. *Journal of Geophysical Research*, *112*, D24S18. https://doi.org/10.1029/2007JD008728

van den Heever, S. C., Carrio, G. G., Cotton, W. R., DeMott, P. J., & Prenni, A. J. (2006). Impacts of nucleating aerosol on Florida storms. Part I: Mesoscale simulations. *Journal of the Atmospheric Sciences*, *63*, 1752–1775.

van den Heever, S. C., Stephens, G. L., & Wood, N. B. (2011). Aerosol Indirect Effects on Tropical Convection Characteristics under Conditions of Radiative-Convective Equilibrium. *Journal of the Atmospheric Sciences*, *68*, 699–718.

Wang, Y., Wan, Q., Meng, W., Liao, F., Tan, H., & Zhang, R. (2011). Long-term impacts of aerosols on precipitation and lightning over the Pearl River Delta megacity area in China. *Atmospheric Chemistry and Physics*, *11*, 12,421–12,436.

Wang, Y., Zhang, R. Y., & Saravanan, R. (2014). Asian pollution climatically modulates mid-latitude cyclones following hierarchical modelling and observational analysis. *Nature Communications*, *5*.

Williams, E., Mushtak, V., Rosenfeld, D., Goodman, S., & Boccippio, D. (2005). Thermodynamic conditions favorable to superlative thunderstorm updraft, mixed phase microphysics and lightning flash rate. *Atmospheric Research*, *76*, 288–306.

Williams, E., Rosenfeld, D., Madden, N., Gerlach, J., Gears, N., Atkinson, L., et al. (2002). Contrasting convective regimes over the Amazon: Implications for cloud electrification. *Journal of Geophysical Research*, *107*(D20), 8082. https://doi.org/10.1029/2001JD000380

Williams, E. R. (1988). The Electrification of Thunderstorms. *Scientific American*, *259*, 88.

Williams, E. R., Rutledge, S. A., Geotis, S. G., Renno, N., Rasmussen, E., & Rickenbach, T. (1992). A Radar and Electrical Study of Tropical Hot Towers. *Journal of the Atmospheric Sciences*, *49*, 1386–1395.

Williams, E. R., & Satori, G. (2004). Lightning, thermodynamic and hydrological comparison of the two tropical continental chimneys. *Journal of Atmospheric and Solar - Terrestrial Physics*, *66*, 1213–1231.

Yuan, T. L., Remer, L. A., Pickering, K. E., & Yu, H. B. (2011). Observational evidence of aerosol enhancement of lightning activity and convective invigoration. *Geophysical Research Letters*, *38*, L04701. https://doi.org/10.1029/2010GL046052